Supporting Information

Optimized Substrates and Measurement Approaches for Raman Spectroscopy of Graphene Nanoribbons

Jan Overbeck*[1,2,3#], Gabriela Borin Barin*[1#], Colin Daniels[4], Mickael Perrin[1], Liangbo Liang[5], Oliver Braun[1,2], Rimah Darawish[1,6], Bryanna Burkhardt[4], Tim Dumslaff[7], Xiao-Ye Wang[7†], Akimitsu Narita[7], Klaus Müllen[7,8], Vincent Meunier[4], Roman Fasel[1,6], Michel Calame[1,2,3] and Pascal Ruffieux*[1]

[1]Empa, Swiss Federal Laboratories for Materials Science and Technology, 8600 Dübendorf, Switzerland

[2]University of Basel, Department of Physics, 4056 Basel, Switzerland

[3]University of Basel, Swiss Nanoscience Institute, 4056 Basel, Switzerland

[4]Rensselaer Polytechnic Institute, Department of Physics, Applied Physics, and Astronomy, Troy, New York 12180, United States

[5]Oak Ridge National Laboratory, Center for Nanophase Materials Sciences, Oak Ridge, Tennessee 37831, United States

[6]University of Bern, Department of Chemistry and Biochemistry, 3012 Bern, Switzerland

[7]Max Planck Institute for Polymer Research, Ackermannweg 10, 55128 Mainz, Germany

[8]Johannes Gutenberg-Universität Mainz, Institute of Physical Chemistry, 55128 Mainz, Germany

[†]current address: State Key Laboratory of Elemento-Organic Chemistry, College of Chemistry, Nankai University, Tianjin 300071, China

[#] These authors contributed equally

corresponding authors: gabriela.borin-barin@empa.ch

jan.overbeck@empa.ch

pascal.ruffieux@empa.ch

Supporting Note 1 – Additional calibrated spectra on Raman optimized (RO)-substrates

To assess the magnitude of the interference enhancement (IE) effect with respect to standard silicon substrates, hybrid devices with adjacent areas of both layer structures were fabricated (see inset of Figure S1a). This allows the direct comparison of Raman intensities obtained from a single scan. Figure S1a shows the enhancement obtained from a device optimized for Raman spectroscopy at an excitation wavelength λ_{ex} = 785 nm (thickness of 114 nm as determined by ellipsometry). Figure S1b shows a device with a significantly thinner oxide, which is beneficial for device applications but still shows significant IE. Note, that the SiO_2/Si substrate itself exhibits an interference effect, which results in enhancement values that differ from what is expected to an interference-free substrate.
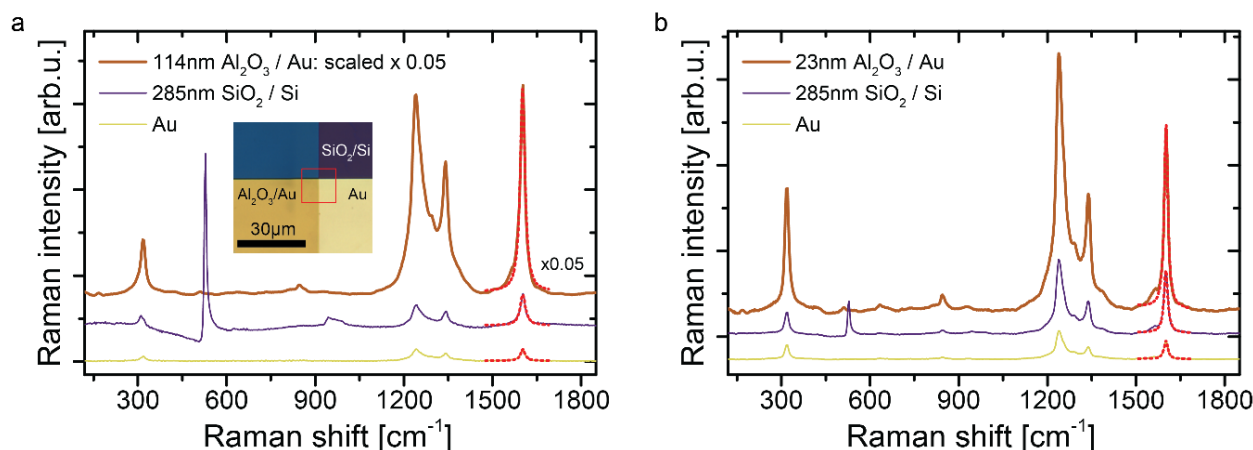

Figure S1. Calibrated enhancement factors for selected oxide thicknesses. a Raman enhancement of the spectrum of 9-AGNR at an oxide thickness of 114 nm optimized for 785 nm excitation. An enhancement of 120 (373) on the RO-substrate is extracted from the G-peak intensity with respect to the signal on SiO_2/Si (Au). Note that the enhanced spectrum had to be scaled by 1/20 to make the peaks apparent for the reference spectra. The inset show how the data are obtained from a single Raman map covering the three substrates. **b** Spectra obtained on thinner (23 nm) oxide as it may be found for atomic-layer-deposited gate oxides in devices, still showing a significant enhancement of 2.3 (9.8). Note the change in relative intensities of the silicon and GNR-signals between a and b, that reflect the variability of GNR growth and transfer. Spectra obtained in air, 100x (NA=0.9) objective.

Supporting Note 2 – Fabrication and modelling of interference enhanced substrates

To experimentally probe the thickness-dependence of the interference effect on RO-substrates, we fabricated a sample with wedged oxide structure, following Solonenko et al. [34]. For this, we used a thick (300 nm) atomic-layer-deposited aluminum oxide layer, which was subsequently etched away while pulling the substrate out of the etchant solution (TMAH-based developer, MF-321). Figure S2a shows an optical micrograph and sketch of the resulting wedge-shaped oxide structure. Raman spectra were acquired via a map-scan for each excitation wavelength (colored outline in a). The G-mode intensity was extracted from a 10 μm averaging window along the scan direction as shown in Figure 3c of the main manuscript. The thickness was calibrated via profilometer measurements.

To model the interference enhancement we first calculate the intensity pattern of the excitation laser in the x-z-plane using the *Wave-Optics* module *COMSOL Multiphysics®* (Figure S2b). Here, we model a layer structure consisting of a SiO_2/Si substrate, a 90 nm thick layer of gold covered by aluminum oxide and air.

We use a wavelength-dependent refractive index for heavily p-doped Si [43], Au [44] and Al_2O_3 [45,46]. This accounts for the wavelength-dependent skin-depth, which shifts the interference maxima to lower values compared to the simple interference model for thin layers, and predicts the first interference maximum at an oxide thickness of $d_{ox} = \lambda/(4*n_{ox}) \approx 118$ nm (80/73 nm) for 785 nm (532/488 nm) excitation.

Further deviations from this simple model result from non-normal incidence for an objective NA = 0.55, which we model *via* a Gaussian beam with a waist w = 0.61*λ/NA. For modeling simplicity, the focal plane is 500 nm above the surface (which is comparable to the experimental uncertainty of the focus adjustment).

Figure S2b shows an RO-substrate with d_{ox} = 40nm, which for λ_{ex} = 488 nm results in an interference maximum at the oxide surface, where the GNR-layer would be located (indicated by a dashed green/black line).

The maximum laser-intensity enhancement $(E/E_0)^2$ = 1.85 for λ_{ex} = 488 nm. Note, that the field penetrates into the gold-layer and that the residual transparency results in a low-intensity interference pattern in the underlying SiO_2-layer. Reducing the metal thickness consequently results in background signal from the silicon substrate, as can be seen for the peak labeled by an asterisk in Figure 2a of the main manuscript.

Figure S2c shows a comparison of the field intensity of an RO-substrate with d_{ox} = 100 nm and a SiO_2/Si substrate for λ_{ex} = 785 nm. This RO-substrate is optimized for maximum intensity at the surface (the GNR layer) for λ_{ex} = 785 nm. In contrast, the layer structure of SiO_2/Si results in an intensity minimum at the surface of the sample, such that a reduced intensity from a deposited GNR-layer is expected. In the top (bottom) panel of Figure S2d we plot the field intensity at the surface reference point (marked with a white cross in b) as a function of z-coordinate (along the orange arrows in Figure S2c) for the Si- (RO-) substrate and the three wavelengths we used. Constructive interference *i.e.* $(E/E_0)^2$>1 at the surface of the SiO_2/Si substrate (z=0) is obtained for λ_{ex} = 532 nm, while the intensity for λ_{ex} = 488 (785) nm is slightly (strongly) reduced. For the RO-substrate with d_{ox} = 100 nm, λ_{ex} = 785 nm is enhanced at the surface while λ_{ex} = 488 / 532 nm show reduced intensity.
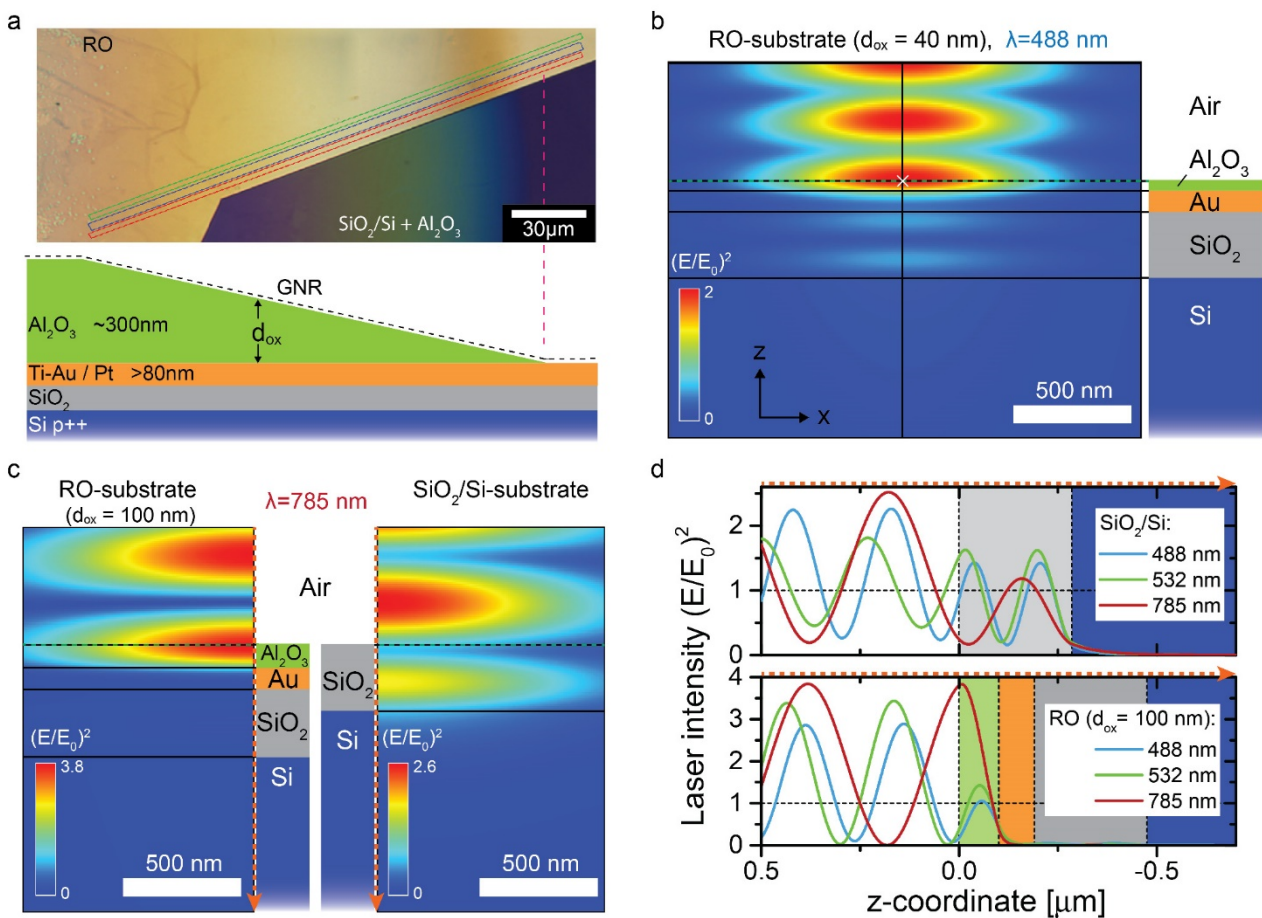
Figure S2. Wedged oxide structure for investigation and modelling of interference effects.
a Optical image with map-overlay and sketch of layer structure used for acquiring oxide thickness dependent spectra. **b** Simulated x-z profile for normalized laser intensity on an RO-substrate with oxide thickness of d_{ox} = 40 nm for λ_{ex} = 488 nm. The layer structure is indicated to the right. The dashed green-black line indicates the layer, where GNRs would be deposited, the white cross the reference position to compare intensity values. **c** Simulated x-z profiles of laser intensity for an RO-substrate optimized for λ_{ex} = 785 nm (d_{ox} = 100 nm, left) and a standard SiO_2/Si-substrate (285 nm SiO_2 thickness). **d** Normalized laser intensity along the centerline indicated by orange arrows in c for an SiO_2/Si substrate (top) and RO-substrate (bottom). The layer structure is color coded in the background as in c.

The overall thickness-dependent evolution of the calculated laser intensity at the RO-substrate surface is plotted in Figure S3a. One observes a non-zero intensity for vanishing oxide thickness, as would be the case for GNRs placed directly on gold, and periodic oscillations of laser intensity as a function of oxide thickness. For general-purpose RO-device substrates ('standard'), an oxide thickness of around 40 nm is used and the oxide layer is etched away except for dedicated areas on the source/drain contact pads (see Figure 3b of the main manuscript). The calculated intensities for these two RO-substrates, the SiO_2/Si-substrate used in our lab, and a reference substrate (RO with d_{ox} = 1 nm) to compare with measurements of GNRs directly on gold are shown in Table S1.

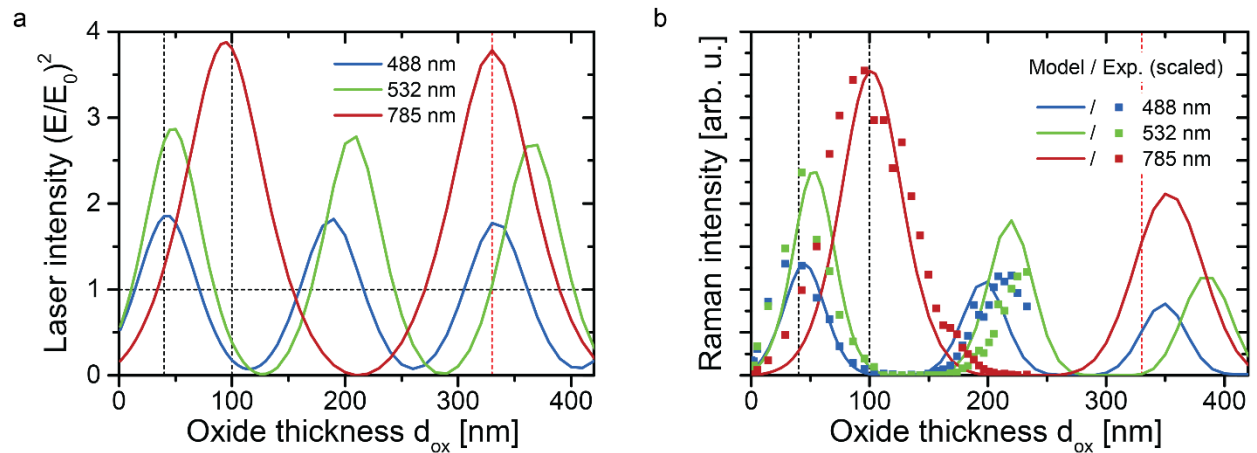| Substrate-type	oxide thickness d_{ox}	Laser-intensity enhancement $(E/E_0)^2$ at the surface for		
		λ_{ex} = 488 nm	λ_{ex} = 532 nm	λ_{ex} = 785 nm
RO – substrate (standard)	40 nm	**1.85**	**2.72**	**1.26**
RO – substrate (opt. 785 nm)	100 nm	0.18	0.39	**3.80**
SiO_2/Si – substrate	285 nm	0.86	**1.23**	0.25
RO – substrate (Au-ref.)	1 nm	0.53	0.57	0.17

Table S1. Comparison of calculated laser intensities.

Figure S3. Modelling of interference enhancement of laser intensity and Raman signal. a Calculated Laser-intensity as a function of aluminum-oxide thickness for RO-substrates. The general-purpose thickness of 40 nm and the thickness d_{ox} = 100 nm optimized for λ_{ex} = 785 nm are indicated by vertical lines. For d_{ox} = 40 nm all wavelengths exhibit enhancement $(E/E_0)^2 > 1$. **b** Modelled Raman intensity of the G-mode (solid lines) compared to experimental intensities (points, scaled to first calculated maximum).

Next, we model the enhancement of the detected Raman intensity. For this, one needs to take into account the self-interference of the Raman shifted (scattered) light[34,35]. In general, this requires a separate analysis of

each Raman mode (each scattered light wavelengths) and significant changes in the peak intensity ratios can be observed[35]. At λ_{ex} = 785 nm and for d_{ox} = 5 – 80 nm, however, we observe enhancement values for the RBLM and G-peak that are within 10% of each other (not shown), suggesting that this effect can be neglected e.g. if identification of low-intensity modes rather than determining their precise intensity ratios is the focus. Nevertheless, we use a simplified model for estimating the Raman signal enhancement of the G-mode. Instead of explicitly modelling the light emission from GNRs at the surface of an RO-substrate, we investigate the interference condition for the Raman-shifted laser light in the same way as the excitation before, and estimate the Raman intensity enhancement $E \propto I_{Laser}*I_{shifted}$. Figure S3b shows the result of this approach for the wavelength pairs 488 nm (529 nm), 532 nm (581 nm), 785 nm (898 nm), where the value in parenthesis is the wavelength corresponding to a Raman shift of 1600 cm^{-1}. We also plot the experimental values for the G-peak intensity from Figure 3c of the main text. The model reproduces the data quite well. In particular, it predicts signal enhancements on the same order of magnitude than what is observed in experiments (see Table S2), despite being idealized in terms of material properties (metal and oxide), surface roughness, and complete absence of plasmonic hotspots.

Experimental substrates	Modelling: oxide thickness d_{ox}	Enhancement: experimental (modelling)		
		λ_{ex} = 488 nm	λ_{ex} = 532 nm	λ_{ex} = 785 nm
RO (23 nm) vs. Au	20 nm – vs. – 1nm			9.8 (10.7)
RO (40 nm) vs. Au	40 nm – vs. – 1nm	11.5 (16.6)	19.5 (31.4)	43.0 (56.5)
RO (114 nm) vs. Au	100 nm – vs. – 1nm			373 (700)

Table S2. Comparison of enhancement from measurements and modelling.

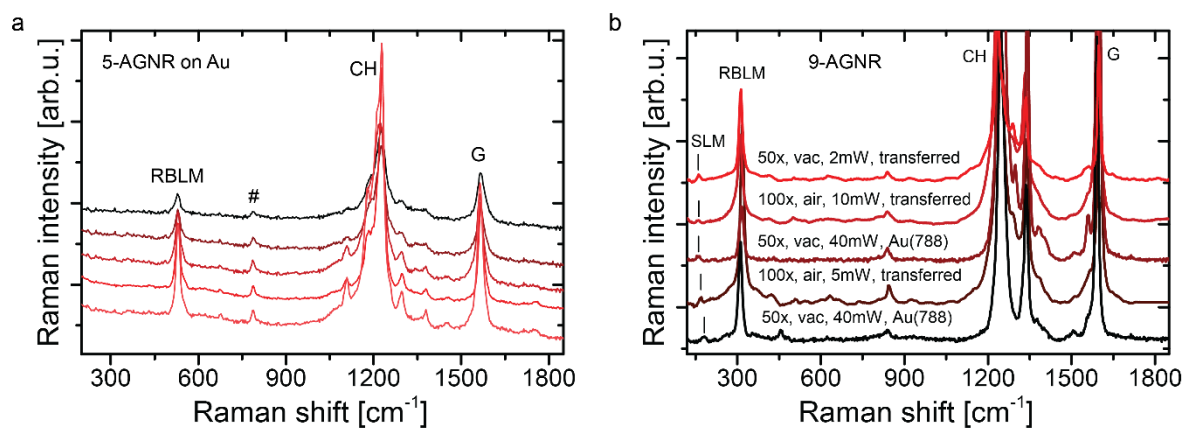## Supporting Note 3 – Raman data on additional samples and normal mode displacements

Figure S4. Additional Spectra. a Spectra from 5-Samples of 5-AGNR on Au growth-substrates. All spectra each constructed via averaging a large area map, exhibit mode '#'. λ_{ex} = 785 nm, 40 mW, in vacuum. No background subtraction. **b** Raman spectra of 9-AGNR sample before and after transfer as indicated. On each sample, the mode at 160-184 cm^{-1} is clearly visible. Excitation wavelength 785 nm.

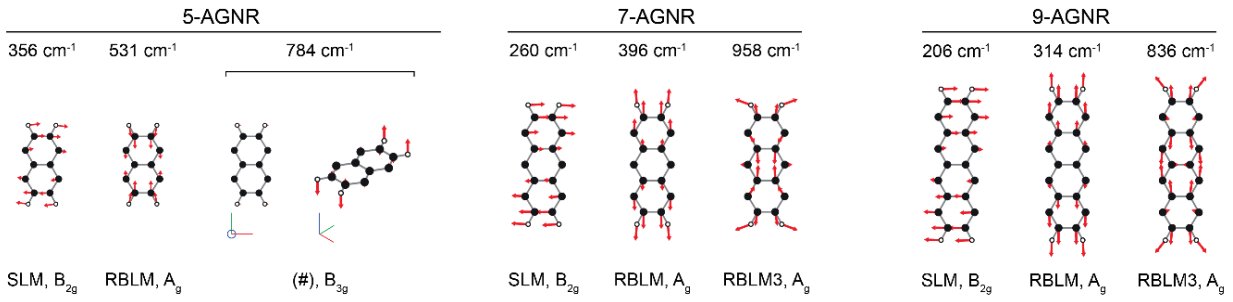| 5-AGNR				7-AGNR			9-AGNR		
356 cm^{-1}	531 cm^{-1}	784 cm^{-1}		260 cm^{-1}	396 cm^{-1}	958 cm^{-1}	206 cm^{-1}	314 cm^{-1}	836 cm^{-1}
SLM, B$_{2g}$	RBLM, A$_g$	(#), B$_{3g}$		SLM, B$_{2g}$	RBLM, A$_g$	RBLM3, A$_g$	SLM, B$_{2g}$	RBLM, A$_g$	RBLM3, A$_g$

Figure S5. Normal mode displacements for low-energy modes. Mode frequencies and symmetries are indicated. For the 5-AGNR, the mode "#" which is experimentally observed at 789 cm^{-1} is tentatively attributed to a mode with B$_{3g}$ symmetry at a Raman shift of 784 cm^{-1}. The out-of-plane vibration can be seen in the side-projections. It becomes Raman allowed for non-normal incidence, which can be due to the GNR-on-substrate morphology and the deviation from normal excitation and detection due to the objective NA=0.55. Normal modes for the low energy 7- and 9-AGNR are shown for comparison. For further calculations we refer to our previous work[12].